

# Quasi-exactly solvable quartic: real algebraic spectral locus

Alexandre Eremenko and Andrei Gabrielov\*

June 15, 2018

## Abstract

We describe the real quasi-exactly solvable spectral locus of the PT-symmetric quartic using the Nevanlinna parametrization.

MSC: 81Q05, 34M60, 34A05.

Keywords: one-dimensional Schrödinger operators, quasi-exact solvability, PT-symmetry, singular perturbation.

Following Bender and Boettcher [3], we consider the eigenvalue problem in the complex plane

$$w'' + (\zeta^4 + 2b\zeta^2 + 2iJ\zeta + \lambda)w = 0, \quad w(te^{-\pi i/2 \pm \pi i/3}) \rightarrow 0, \quad t \rightarrow +\infty, \quad (1)$$

where  $J$  is a positive integer. This problem is quasi-exactly solvable [3]: there exist  $J$  elementary eigenfunctions  $w = p_n(\zeta) \exp(-i\zeta^3/3 - ib\zeta)$ , where  $p_n$  is a polynomial of degree  $n = J - 1$ .

When  $b$  is real, the problem is PT-symmetric. By the change of the independent variable  $z = i\zeta$ , (1) is equivalent to

$$-y'' + (z^4 - 2bz^2 + 2Jz)y = \lambda y, \quad y(te^{\pm \pi i/3}) \rightarrow 0, \quad t \rightarrow +\infty. \quad (2)$$

Polynomial  $h$  in the exponent of an elementary eigenfunction  $y(z)$  is  $h(z) = z^3/3 - bz$ . The *spectral locus*  $Z_J$  is defined as

$$\{(b, \lambda) \in \mathbf{C}^2 : \exists y \neq 0 \text{ satisfying (2)}\}.$$

---

\*Both authors are supported by NSF grant DMS-1067886.

The real spectral locus  $Z_J(\mathbf{R})$  is  $Z_J \cap \mathbf{R}^2$ . The quasi-exactly solvable spectral locus  $Z_J^{QES}$  is the set of all  $(b, \lambda) \in Z_J$  for which there exists an elementary solution  $y$  of (2). This is a smooth irreducible algebraic curve in  $\mathbf{C}^2$ , [1, 2]. In this paper we describe  $Z_J^{QES}(\mathbf{R}) = Z_J^{QES} \cap \mathbf{R}^2$ . We prove a result announced in [6]:

**Theorem 1.** For  $n \geq 0$ ,  $Z_{n+1}^{QES}(\mathbf{R})$  consists of  $[n/2] + 1$  disjoint analytic curves  $\Gamma_{n,m}$ ,  $0 \leq m \leq [n/2]$  (analytic embeddings of  $\mathbf{R}$  to  $\mathbf{R}^2$ ).

For  $(b, \lambda) \in \Gamma_{n,m}$ , the eigenfunction has  $n$  zeros,  $n - 2m$  of them real.

If  $n$  is odd, then  $b \rightarrow +\infty$  on both ends of each curve  $\Gamma_{n,m}$ . If  $n$  is even, then the same holds for  $m < n/2$ , but on the ends of  $\Gamma_{n,n/2}$  we have  $b \rightarrow \pm\infty$ .

If  $(b, \lambda) \in \Gamma_{n,m}$ ,  $(b, \mu) \in \Gamma_{n,m+1}$  and  $b$  is sufficiently large, then  $\mu > \lambda$ .

This theorem establishes the main features of  $Z_{n+1}^{QES}(\mathbf{R})$  which can be seen in the computer-generated figure in [3]. Similar results were proved in [5] for two other PT-symmetric eigenvalue problems.

Our theorem parametrizes all polynomials  $P$  of degree 4 with the property that the differential equation  $y'' + Py = 0$  has a solution with  $n$  zeros,  $n - 2m$  of them real [10, 7, 5].

Suppose that  $(b, \lambda) \in Z_J^{QES}(\mathbf{R})$ . Then the corresponding eigenfunction  $y$  of (2) can be always chosen real. Let  $y_1$  be a real solution of the differential equation in (2) normalized by  $y_1(x) \rightarrow 0$  as  $x \rightarrow +\infty$ ,  $x \in \mathbf{R}$ . Then  $y_1$  is linearly independent of  $y$ . Consider the meromorphic function  $f = y/y_1$ . This function has no critical points in  $\mathbf{C}$ , and the only singularities of  $f^{-1}$  are six logarithmic branch points. A meromorphic function in  $\mathbf{C}$  with no critical points and whose inverse has finitely many logarithmic singularities is called a *Nevanlinna function*. All Nevanlinna functions  $f$  arise from differential equations  $y'' + Py = 0$ , where  $P$  is a polynomial by the above construction:  $f$  is a ratio of two linearly independent solutions of the differential equation.

Consider the sectors

$$S_j = \{te^{i\theta} : t > 0, |\theta - \pi j/3| < \pi/6\}, \quad j = 0, \dots, 5.$$

The subscript  $j$  in  $S_j$  will be always understood as a residue modulo 6. Function  $f$  has asymptotic values  $\infty, 0, c, 0, \bar{c}, 0$  in the sectors  $S_0, \dots, S_5$ , where  $c \in \overline{\mathbf{C}}$ . It is known that  $f$  must have at least 3 distinct asymptotic values [9], so  $c \neq 0, \infty$ . Function  $f$  is defined up to multiplication by a non-zero real number, so we can always assume that  $c = e^{i\beta}$ ,  $0 \leq \beta \leq \pi$ , where the points 0 and  $\pi$  can be identified. The asymptotic value  $c$  is called the *Nevanlinna*

parameter. There is a simple relation between  $c$  and the Stokes multipliers [11, 8].

The sectors  $S_j$  correspond to logarithmic singularities of the inverse function  $f^{-1}$ . Thus  $f^{-1}$  has 6 logarithmic singularities that lie over 4 points if  $c \neq \bar{c}$ , or over 3 points if  $c = \bar{c}$ .

The map  $(b, \lambda) \mapsto \beta \pmod{\pi}$ ,  $Z_J^{QES}(\mathbf{R}) \rightarrow \mathbf{R}$  is analytic and locally invertible [11, 2], so  $\beta$  can serve as a local parameter on the real QES spectral locus. To obtain a global parametrization one needs suitable charts on  $Z_J^{QES}(\mathbf{R})$ , where this map is injective.

To recover  $f$ , one has to know the asymptotic value  $c$  and one more piece of information, a certain cell decomposition of the plane described below. Once  $f$  is known,  $b$  and  $\lambda$  are found from the formula

$$\frac{f'''}{f'} - \frac{3}{2} \left( \frac{f''}{f'} \right)^2 = -2(z^4 - 2bz^2 + 2Jz - \lambda). \quad (3)$$

Now we describe, following [4], the cell decompositions needed to recover  $f$  from  $c$ . Suppose first that  $c \notin \mathbf{R}$ .

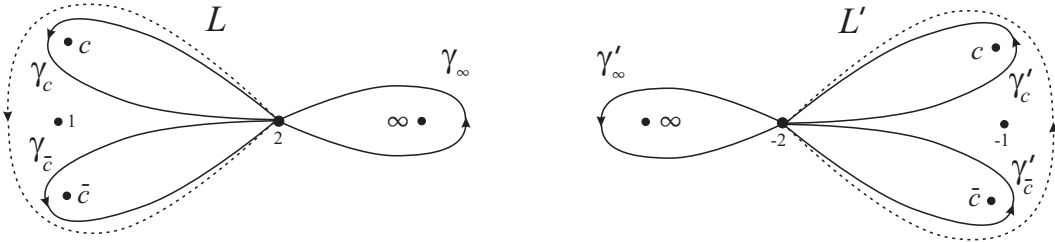


Fig. 1. Cell decompositions  $\Phi$  and  $\Phi'$  of the sphere (solid lines).

Consider the cell decomposition  $\Phi$  of the Riemann sphere  $\overline{\mathbf{C}}$  shown by solid lines in the left part of Fig. 1. It consists of one vertex at the point 2, three edges (loops  $\gamma_c$ ,  $\gamma_{\bar{c}}$  and  $\gamma_\infty$  around non-zero asymptotic values) and four faces (cells of dimension 2). The faces are labeled by the asymptotic values 0,  $c$ ,  $\bar{c}$ ,  $\infty$ . Label 0 is not shown in the picture. The face labeled 0 is the unbounded region in the picture. (The point 1 in the figure is neither a label, nor a part of the cell decomposition. It will be needed, together with the dashed line  $L$ , for the limit at  $\beta = 0$ .) As

$$f : \mathbf{C} \setminus f^{-1}(\{0, \infty, c, \bar{c}\}) \rightarrow \overline{\mathbf{C}} \setminus \{0, \infty, c, \bar{c}\}$$

is a covering map, the cell decomposition  $\Phi$  pulls back to a cell decomposition  $\Psi$  of the plane.

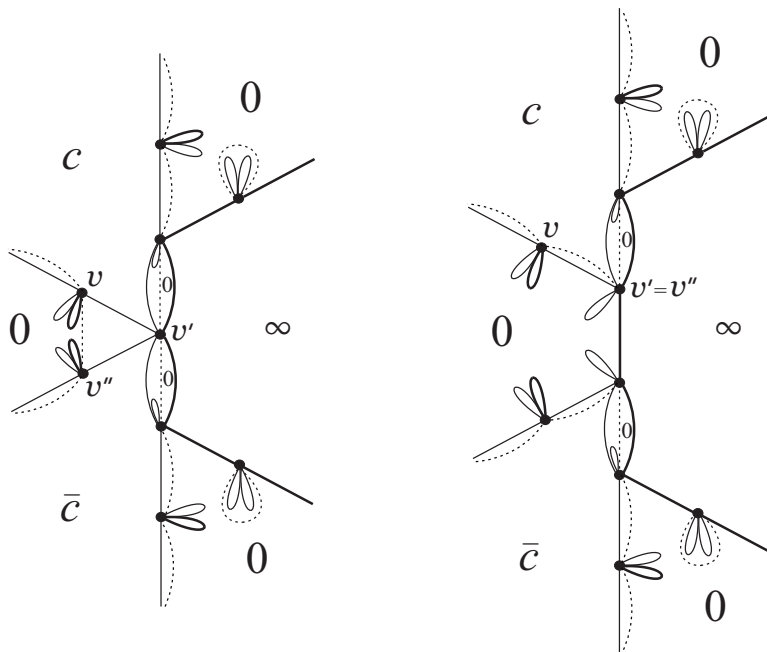


Fig. 2. Two examples of the cell decomposition  $\Psi$  of the plane (solid lines). Both eigenfunctions have two zeros, none of them real.

Examples of  $\Psi$  are shown with solid lines in Figs. 2 and 4 (left). The faces of  $\Psi$  are labeled with the same labels as their images. Non-zero labels of bounded faces are omitted in the picture. The reader can restore them from the condition that labels around a vertex must be in the same cyclic order as in Fig. 1 (left, solid lines). The labeled cell decomposition  $\Psi$  defines  $f$  up to a pre-composition with an affine map of  $\mathbf{C}$ . Two cell decompositions define the same  $f$  if they can be obtained from each other by a homeomorphism of the plane preserving orientation and the labels. Such cell decompositions are called equivalent.

By replacing multiple edges of the 1-skeleton of  $\Psi$  with single edges and removing the loops, we obtain a simpler cell decomposition  $T$  whose 1-skeleton is a tree, which we denote by the same letter  $T$ . The cell decomposition  $\Psi$  is uniquely recovered from its tree  $T$  embedded in the plane, [4]. The faces of  $T$  are asymptotic to the sectors  $S_j$  and the label of each face is the asymptotic

value in  $S_j$ . Two faces with a common edge cannot have the same label. The cell decomposition  $T$  is invariant under the reflection in the real axis, with simultaneous interchange of  $c$  and  $\bar{c}$ . It is easy to classify all possible embedded planar trees  $T$  with labeled faces that satisfy these properties. They depend on two integer parameters  $k$  and  $l \geq 0$ . These trees form two families,  $X_{k,l}$ ,  $k \geq 0, l \geq 0$  and  $X_{k,l}$ ,  $k < 0, l \geq 0$ , shown in Fig. 3. Integers  $|k|$  and  $l$  are the numbers of edges between ramification vertices, as shown in Fig. 3.

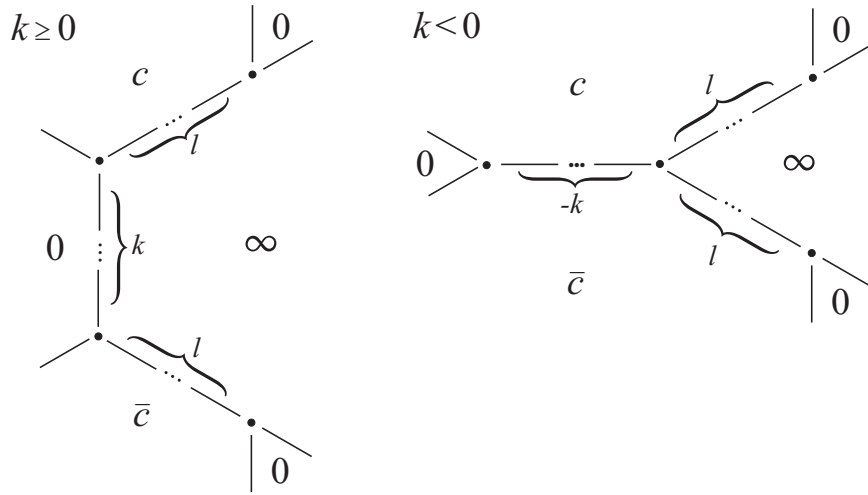


Fig. 3. Trees  $X_{k,l}$ .

Cell decompositions in Fig. 2 (solid lines) correspond to the trees  $X_{0,1}$  and  $X_{1,1}$ . Cell decomposition in the left part of Fig. 4 (solid lines) corresponds to the tree  $X_{-1,1}$  in the right part of Fig. 4.

Parameters of the trees  $X_{k,l}$  can be interpreted as follows:

$$k^- := \min\{-k, 0\}$$

is the number of real zeros of  $f$ , and  $2l$  is the number of non-real zeros. So the total number of zeros is  $n = 2l + k^-$ .

Functions  $f$  corresponding to the trees  $X_{k,l}$ ,  $k \geq 0$ , have  $2l$  zeros, none of them real. Zeros of the eigenfunction  $y$  coincide with those of  $f$ .

For given  $n$ , the number of trees  $X_{k,l}$  with  $k < 0$ ,  $2l - k = n$  is

$$(n + 1)/2 \text{ when } n \text{ is odd, and } n/2 \text{ when } n \text{ is even.} \quad (4)$$

Every tree  $X_{k,l}$  and every  $\beta \in (0, \pi)$  defines a meromorphic function  $f$  satisfying (3) with  $J = 2l + k^- + 1$  and some  $(b, \lambda)$  depending on  $\beta, k$  and  $l$ . This follows from a result of Nevanlinna [9], see also [4]. From this function  $f$ , the coordinates of a point  $(b, \lambda)$  on the real QES spectral locus are recovered from the Schwarz equation (3). Thus we have a map  $F : (T, \beta) \mapsto (b, \lambda)$  which we call the *Nevanlinna map*. This map is of highly transcendental nature: construction of  $f$  from  $T$  and  $\beta$  involves the uniformization theorem. We refer to [4, 5, 9] for details.

Each of the trees from our classification defines a chart of  $Z_J^{QES}(\mathbf{R})$ . To obtain the global parametrization of  $Z_J^{QES}(\mathbf{R})$ , we only have to find out how these charts are pasted together. We will see that the boundaries of our charts correspond to the values  $c = \pm 1$ . When  $c$  is real, we can use, instead of  $\Phi$ , the cell decomposition  $\Phi_1$  of the sphere with two loops,  $\gamma_\infty$  and the loop  $L$  around  $c$  shown with the dashed line in the left part of Fig. 1.

*Proof of Theorem 1.* We begin with the charts  $X_{k,l}$ ,  $k < 0$ . We show that in these charts the limits as  $\beta \rightarrow 0, \pi$  do not belong to the spectral locus. This is proved by the arguments similar to those in [5, Thm. 4.1].

**Lemma 1.** *For  $k < 0$  and  $l \geq 0$ , the limit of the Nevanlinna map is*

$$\lim_{\beta \rightarrow 0} F(X_{k,l}, \beta) = \infty.^1$$

*Proof.* When  $\beta \rightarrow 0$ , we have  $c \rightarrow 1$ ,  $\bar{c} \rightarrow 1$ . Suppose by contradiction that  $F(X_{k,l}, \beta)$  has a limit  $(b_0, \lambda_0)$ . Then there is a limit function  $f_0$ , a solution of the Schwarz equation (3) with these parameters  $b_0$  and  $\lambda_0$ . Meromorphic function  $f_0$  has three asymptotic values,  $0, 1, \infty$ , and we are going to find the corresponding cell decomposition. Let  $\Phi_1$  be the cell decomposition of the Riemann sphere with one vertex at the point 2 and two loops,  $\gamma_\infty$  and  $L$  (see Fig. 1, left). Let  $\Psi_1 = f^{-1}(\Phi_1)$ .

It is easy to construct  $\Psi_1$  from the original cell decomposition  $\Psi$ . First, removing preimages of  $\gamma_c$  and  $\gamma_{\bar{c}}$ , we obtain the cell decomposition  $\Psi_\infty$ , the preimage of the loop around  $\infty$  in  $\Phi$ . It is shown with the bold solid lines in Fig. 4.

Next, for each vertex  $v$  of  $\Psi$  consider the path  $L_v$  consisting of the edge of  $f^{-1}(\gamma_c)$  starting at  $v$  and ending at some vertex  $v'$ , followed by the edge of  $f^{-1}(\gamma_{\bar{c}})$  starting at  $v'$  and ending at some vertex  $v''$ . Then the edge of  $f^{-1}(L)$

---

<sup>1</sup>Here  $\infty$  refers to a point added to the  $(b, \lambda)$ -plane in the one-point compactification.

from  $v$  to  $v''$  is homotopic to  $L_v$  in the complement of  $\Psi_\infty$ . The new edges are shown with dashed lines in Fig. 4. The resulting cell decomposition is equivalent to  $\Psi_1$ .

Let  $V$  be the set of the vertices of  $\Psi$  contained in the boundary of the sector  $S_3$ . It is connected to the rest of the vertices of  $\Psi$  only at one vertex ( $v'$  in Fig. 4, left) which is also at the boundary of both sectors  $S_2$  and  $S_4$ . The dashed line replacing the edges of  $\Psi$  that connect  $v'$  to the two adjacent vertices of  $V$  ( $v$  and  $v''$  in Fig 4, left), goes from  $v$  to  $v''$ . All other dashed lines connect the vertices of  $V \setminus \{v'\}$  with the other vertices from the same set. Hence  $V \setminus \{v'\}$  is the set of vertices of a connected component of the 1-skeleton of the cell decomposition  $\Psi_1$ . This contradicts our assumption that  $\Psi_1 = f_0^{-1}(\Phi_1)$ , since the 1-skeleton of  $f_0^{-1}(\Phi_1)$  must be connected. This contradiction proves the lemma.

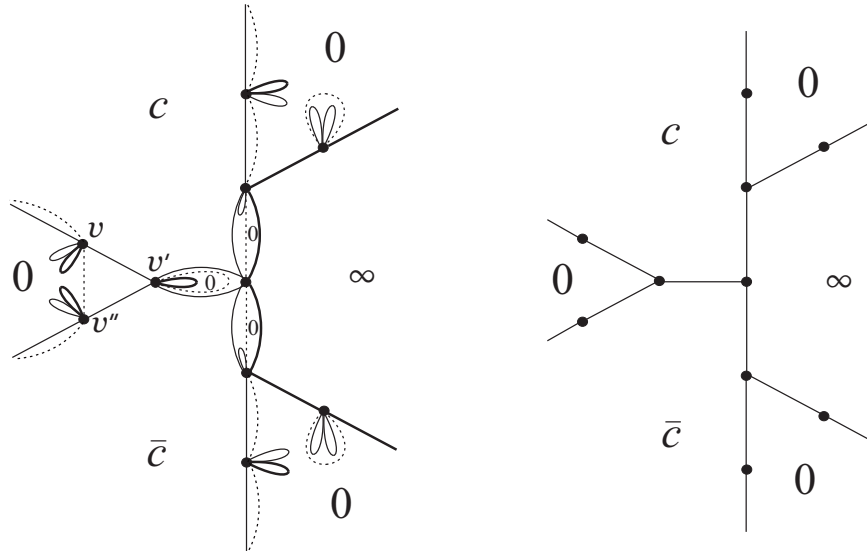


Fig. 4. A cell decomposition  $\Psi$  (solid lines) and the corresponding tree  $X_{-1,1}$ . Eigenfunction has one real and two non-real zeros.

*Remark.* Consider all meromorphic functions with no critical points and at most 6 asymptotic values. These functions  $f$  are defined by their asymptotic values and cell decompositions. Assume that one vertex  $v_0$  of  $\Psi$  is placed at  $z = 0$  and normalize so that  $f'(0) = 1$ . The class of normalized functions

obtained in this way is *compact* [12]. Let  $f_\nu \rightarrow f_0$  be a converging sequence.<sup>2</sup> The 1-skeletons of the corresponding cell decompositions  $\Psi(\nu)$  converge to the 1-skeleton of the cell decomposition  $\Psi(0)$  as embedded graphs with a marked vertex. If two asymptotic values collide in the limit, one has to use the procedure described in the proof of Lemma 1: replacing two loops by one loop. The limiting cell decomposition obtained in Lemma 3 suggests that the eigenvalue problem (2) tends to a harmonic oscillator when  $c \rightarrow 1$ , the fact we'll later prove by different arguments.

**Lemma 2.** *For  $k < 0$  and  $l \geq 0$ ,*

$$\lim_{\beta \rightarrow \pi} F(X_{k,l}, \beta) = \infty.$$

*Proof.* When  $\beta \rightarrow \pi$ , we have  $c \rightarrow -1$ ,  $\bar{c} \rightarrow -1$ . Suppose by contradiction that  $F(X_{k,l}, \beta)$  has a limit  $(b_0, \lambda_0)$ . Then there is a limit function  $f_0$ , a solution of the Schwarz equation (3) with these parameters  $b_0$  and  $\lambda_0$ . Meromorphic function  $f_0$  has three asymptotic values,  $0, -1, \infty$ , and we are going to find the corresponding cell decomposition.

To do this, it is convenient to choose another cell decomposition  $\Phi'$  of the Riemann sphere, shown in the right part of Fig. 1 (solid lines). When  $c \rightarrow -1$ ,  $\Phi'$  collapses to  $\Phi'_{-1}$  where the two loops  $\gamma'_c$  and  $\gamma'_{\bar{c}}$  are replaced with a single loop  $L'$  around  $-1$  (dashed line in Fig. 1, right).

We need the transition formula from  $\Psi = f^{-1}(\Phi)$  to  $\Psi' = f^{-1}(\Phi')$ . This formula is obtained by combining the two decompositions (see Fig. 5) and expressing the loops of  $\Phi'$  in terms of the loops of  $\Phi$ .

---

<sup>2</sup>Uniform convergence on compact subsets in the plane, with respect to the spherical metric in the target sphere.



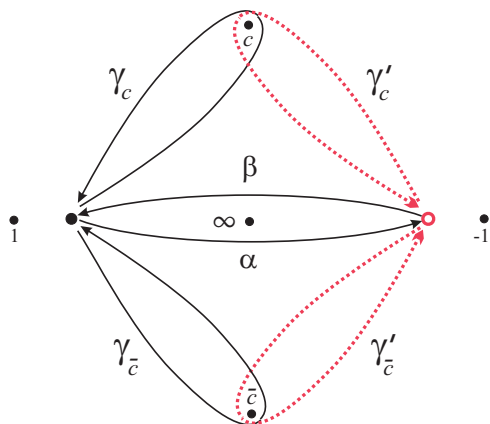


Fig. 5. Two cell decompositions of Fig. 1 combined.

The formulas, using notations in Fig. 5, are:

$$\gamma_\infty = \alpha \beta, \quad \gamma'_\infty = \beta \alpha, \quad \gamma'_c = \beta \gamma_c \beta^{-1}, \quad \gamma'_{\bar{c}} = \alpha^{-1} \gamma_{\bar{c}} \alpha. \quad (5)$$

Here the product should be read left to right. Similar formulas were obtained in [5] in the proof of Theorem 4.1. Application of these transition formulas to the cell decomposition  $\Psi$  of type  $X_{-1,1}$  is illustrated in Figs. 6,7.

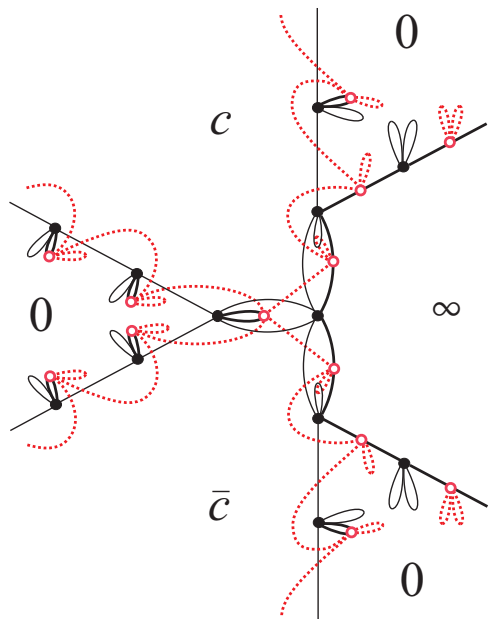


Fig. 6. Transition formulas (5) applied to the cell decomposition in Fig. 4.

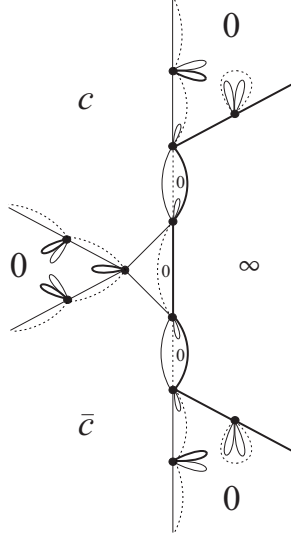


Fig. 7. Cell decomposition  $\Psi'$ .

The same arguments as in Lemma 1 show that the 1-skeleton of the degeneration  $\Psi'_{-1}$  of  $\Psi'$  as  $\beta \rightarrow \pi$  is not connected. This proves the lemma.

Lemmas 1 and 2 show that for  $k < 0$ , the charts  $X_{k,m}$  with  $2m - k = n$  cover connected components of  $Z_{n+1}^{QES}(\mathbf{R})$ , each parametrized by  $\beta \in (0, \pi)$ . We call these components  $\Gamma_{n,m}$ . These are simple disjoint analytically embedded curves in  $\mathbf{R}^2$ .

When  $\beta \rightarrow 0, \pi$  we must have  $b \rightarrow \pm\infty$ . We'll show below that  $b \rightarrow +\infty$  on both ends of  $\Gamma_{n,m}$  when  $k > 0$ .

When  $n$  is odd (that is  $J$  is even), these curves  $\Gamma_{n,m}$  constitute the whole spectral locus  $Z_{n+1}^{QES}(\mathbf{R})$ .

Now consider the part of the spectral locus covered by the charts  $X_{k,l}$ ,  $k \geq 0$ . This part is present only when  $n = 2l$  is even.

**Lemma 3.** *For  $k \geq 0$  and  $l \geq 0$ , we have*

$$\lim_{\beta \rightarrow \pi} F(X_{k,l}, \beta) = \lim_{\beta \rightarrow 0} F(X_{k+1,l}, \beta). \quad (6)$$

and

$$\lim_{\beta \rightarrow 0} F(X_{0,l}, \beta) = \infty. \quad (7)$$

*Proof of Lemma 3.* This is similar to the arguments in Lemmas 1 and 2. Computation is illustrated in Figs. 2, 8, 9 and 10.

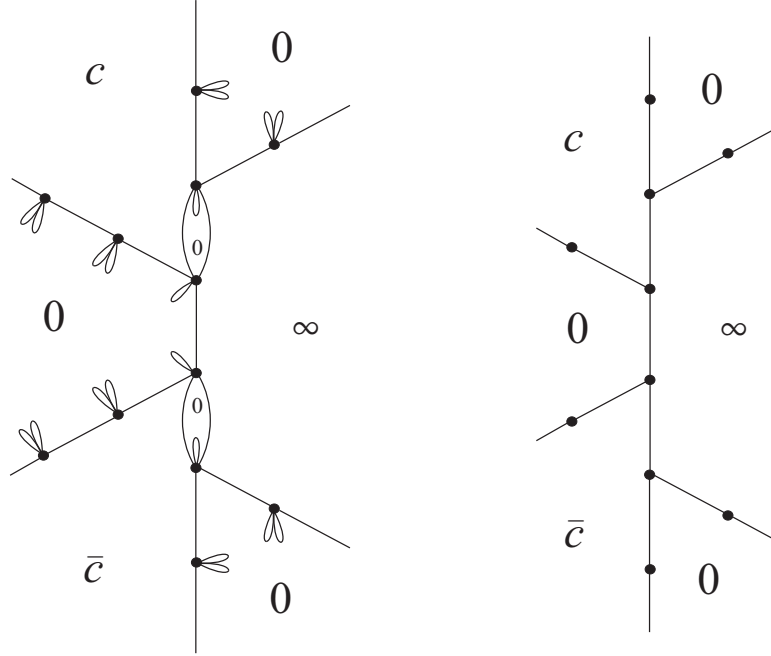


Fig. 8. Cell decomposition  $\Psi$  corresponding to  $X_{1,1}$ .

In the left part of Fig. 8 we use  $\Psi$  from Fig. 2, right. It corresponds to the tree  $X_{1,1}$  in Fig. 8, right. In Fig. 9 the circles denote the vertices of  $\Psi'$  (preimages of the vertex of  $\Phi'$ ) and the dotted lines correspond to the preimages of  $\gamma'_c$  and  $\gamma'_{\bar{c}}$  determined from (5). The preimages of  $\gamma_\infty$  and  $\gamma'_\infty$  coincide. They are shown with the bold solid line. Removing the preimages of  $\gamma_c$  and  $\gamma_{\bar{c}}$  (thin solid lines in Fig. 9) and the vertices of  $\Psi$ , we obtain the cell decomposition  $\Psi'$  shown in Fig. 10 (left) corresponding to the tree  $X_{2,1}$  (right).

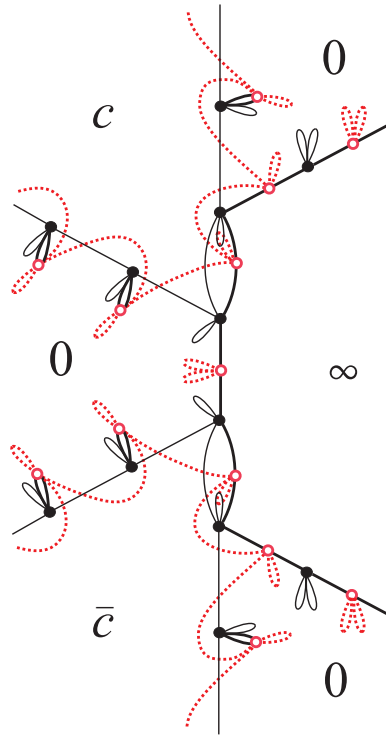


Fig. 9. Passing from  $\Psi$  to  $\Psi'$ .

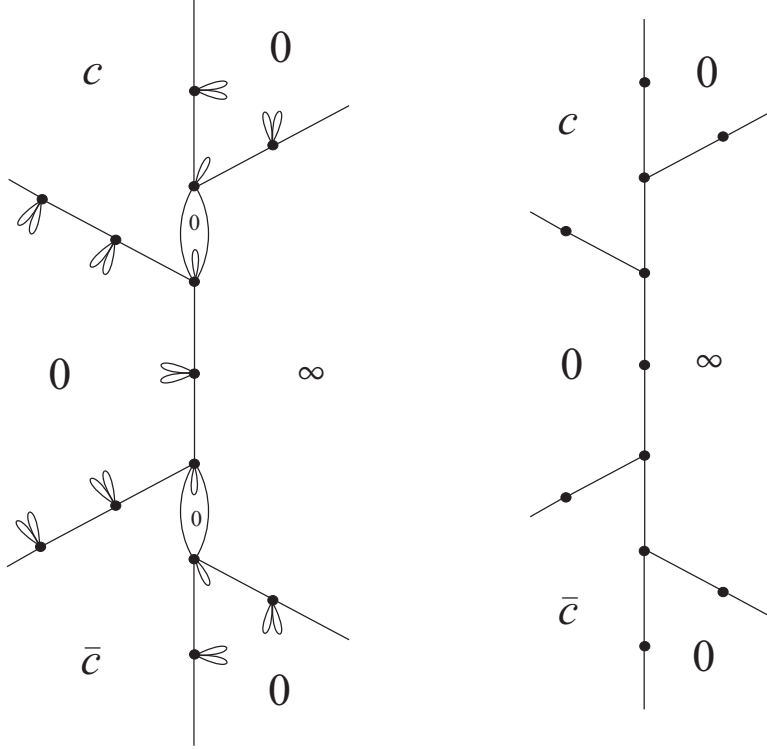


Fig. 10. Cell decomposition  $\Psi'$  corresponding to the tree  $X_{2,1}$ .

Thus, for  $k \geq 0$ , the cell decomposition  $\Psi'_{-1}$  of the plane obtained from  $X_{k,l}$  in the limit  $\beta \rightarrow \pi$  as the preimage of  $\Phi'_{-1}$  is equivalent to the cell decomposition  $\Psi_1$  obtained from  $X_{k+1,l}$  in the limit  $\beta \rightarrow 0$  as the preimage of  $\Phi_1$ . Since  $\Phi'_{-1} = -\Phi_1$ , Nevanlinna theory implies that the corresponding functions  $f$  and  $f'$  satisfy  $f' = -f$ . Hence these two functions correspond to the same point of  $Z_j^{QES}(\mathbf{R})$ .

The proof of (7) is similar to that of Lemma 1. This completes the proof of the lemma.

Now we continue the proof of Theorem 1.

For even  $n = 2l$ , charts  $X_{k,l}$ ,  $k \geq 0$  parametrize segments of one curve in the real QES spectral locus, and we call this curve  $\Gamma_{n,n/2}$ . We parametrize the curve  $\Gamma_{n,n/2}$  by the real line, so that the number  $k$  decreases, thus the right end of  $\Gamma_{n,n/2}$  is parametrized by the chart  $X_{0,n/2}$ . So when the parameter  $t \in \mathbf{R}$  on  $\Gamma_{n,n/2}$  tends to  $+\infty$ , the asymptotic value  $c = \exp(i\beta)$  tends to 1. On the other hand, when  $t \rightarrow -\infty$  on  $\Gamma_{n,n/2}$  the asymptotic value  $c$  does

not have a limit; it oscillates, passing each point of the unit circle infinitely many times.

The curves  $\Gamma_{n,m}$  are disjoint. Indeed, different cell decompositions give different functions  $f$ . This proves the first two statements of Theorem 1.

Now we deal with the asymptotic behavior of our curves  $\Gamma_{n,m}$ . We use the rescaling of (2) as in [6]. The QES spectral locus is defined by a polynomial equation  $Q_{n+1}(b, \lambda) = 0$  which is of degree  $n + 1$  in  $\lambda$ . So on a ray  $b > b_0$  there are  $n + 1$  branches  $\lambda_j(b)$ . In [6, Eq. (25)], we found that all  $\lambda_j$  have asymptotics  $\lambda(b) \sim b^2 + O(\sqrt{b})$ ,  $b \rightarrow \infty$ , and as  $b \rightarrow +\infty$ , each QES eigenfunction  $y_j$  tends to some eigenfunction  $Y_\ell$  of the harmonic oscillator

$$-Y'' + 4z^2Y = \mu Y, \quad Y(it) \rightarrow 0, \quad t \rightarrow \pm\infty. \quad (8)$$

The eigenvalues of this harmonic oscillator are  $\mu_\ell = 2(2\ell + 1)$ ,  $\ell = 0, 1, \dots$

Only one of the eigenfunctions  $y_j$  can tend to a given  $Y_\ell$ , and the corresponding eigenvalue satisfies

$$\lambda_j(b) = b^2 + (\mu_\ell - 2J + o(1))\sqrt{b}, \quad b \rightarrow +\infty.$$

It follows that all  $\lambda_j$  are real. The graph of each  $\lambda_j$  is a part of a curve  $\Gamma_{n,m}$ , and each  $\Gamma_{n,m}$  has only two ends.

Now we consider the degeneration of the  $X_{0,l}$  chart with  $l \geq 0$ , the chart which parametrizes the right end of  $\Gamma_{n,n/2}$ ,  $n = 2l$ . On the left end of  $\Gamma_{n,n/2}$ , where  $t \rightarrow -\infty$  in the parametrization described after Lemma 3, there are infinitely many points  $\Gamma_{n,n/2}(t_k)$  which belong to the real QES locus, and where the asymptotic value  $c$  is real. It was proved in [6] that these are exactly those points where  $Z_J^{QES}(\mathbf{R})$  crosses the non-quasi-exactly solvable part of  $Z_J(\mathbf{R})$ , and these points correspond to  $b_k \rightarrow -\infty$ .

So only on one end of  $\Gamma_{n,n/2}$  (where  $t \rightarrow +\infty$ ) we can have  $b \rightarrow +\infty$ . On the other hand, each  $\Gamma_{n,m}$ ,  $m < n/2$  contains at most two graphs of  $\lambda_j$ . According to (4), the total number of these graphs  $\lambda_j$  is  $n + 1$ , and the total number of curves  $\Gamma_{n,m}$  is  $(n + 1)/2$  when  $n$  is odd, and  $n/2 + 1$  when  $n$  is even. It follows that, when  $n$  is odd, each  $\Gamma_{n,m}$  contains two graphs of  $\lambda_j$ . When  $n$  is even, each  $\Gamma_{n,m}$  except one contains two graphs of  $\lambda_j$ , while the exceptional component  $\Gamma_{n,n/2}$  contains one graph of  $\lambda_j$ .

Thus  $b \rightarrow +\infty$  as  $c \rightarrow \pm 1$  in the  $X_{k,l}$ -charts with  $k < 0$ , which proves the third statement of Theorem 1. To prove the last statement, we study zeros of the eigenfunctions as  $b \rightarrow +\infty$ .

The eigenfunction  $Y_\ell$  of (8) corresponding to the eigenvalue  $\mu_\ell$  has exactly  $\ell$  zeros on  $i\mathbf{R}$  and no other zeros in  $\mathbf{C}$ . One of these zeros is real iff  $\ell$  is odd.

The trees corresponding to  $Y_\ell$  are constructed similarly to those corresponding to  $y$ , using the two loop cell decomposition of the sphere, consisting of  $\gamma_\infty$  and the dashed loop in Fig. 1, left.

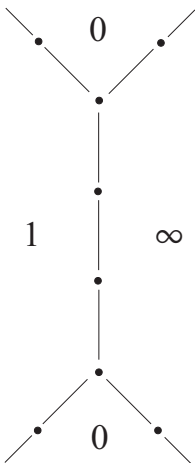


Fig. 11. The tree corresponding to  $Y_3$ .

For general results on convergence of Nevanlinna functions like our  $f$  we refer to [12].

When  $b \rightarrow +\infty$ , each QES eigenvalue  $\lambda(b)$  must tend to some  $\mu_\ell$ , and the corresponding QES eigenfunction tends to  $Y_\ell$ . Suppose that  $\lambda(b) \in \Gamma_{n,m}$  with  $m < n/2$ . Then the tree corresponding to  $\lambda(b)$  is  $X_{k,m}$ ,  $k < 0$ ,  $2m - k = n$ . From the arguments in the proofs of Lemmas 1 and 2 (see Figs. 4, 7), degeneration of the cell decomposition  $\Psi$  corresponding to such a tree has a connected component with  $2m$  bounded faces when  $\beta \rightarrow 0$  and with  $2m + 1$  bounded faces when  $\beta \rightarrow \pi$ . This implies that the corresponding eigenfunction can only converge to  $Y_{2m}$  as  $\beta \rightarrow 0$  and to  $Y_{2m+1}$  as  $\beta \rightarrow \pi$ .

If  $n$  is odd, these curves constitute the whole QES locus. If  $n$  is even, there is one more branch  $\lambda(b)$  of the QES locus for large positive  $b$ , the right end of  $\Gamma_{n,n/2}$  corresponding to the tree  $X_{0,n/2}$ . From the proof of Lemma 3 (see Fig. 2, left) degeneration of the cell decomposition  $\Psi$  corresponding to such a tree has a connected component with  $n$  bounded faces when  $\beta \rightarrow 0$ . This implies that the corresponding eigenfunction can only converge to  $Y_n$ .

So the ordering of the ends of the curves  $\Gamma_{n,m}$  corresponds to the natural ordering of the first  $n + 1$  eigenvalues of the harmonic oscillator. This completes the proof.

## References

- [1] P. Alexandersson and A. Gabrielov, On eigenvalues of the Schrödinger operator with a complex-valued polynomial potential, arXiv:1011.5833.
- [2] I. Bakken, A multiparameter eigenvalue problem in the complex plane, *Amer. J. Math.* 99 (1977), no. 5, 1015–1044.
- [3] C. Bender and S. Boettcher, Quasi-exactly solvable quartic potential, *J. Phys. A* 31 (1998), no. 14, L273–L277.
- [4] A. Eremenko and A. Gabrielov, Analytic continuation of eigenvalues of a quartic oscillator, *Comm. Math. Phys.* 287 (2009), no. 2, 431–457,
- [5] A. Eremenko and A. Gabrielov, Singular perturbation of polynomial potentials in the complex domain with applications to PT-symmetric families, arXiv:1005.1696, to appear in *Moscow Math. J.*
- [6] A. Eremenko and A. Gabrielov, Quasi-exactly solvable quartic: elementary integrals and asymptotics, arXiv:1104.2305.
- [7] A. Eremenko and A. Merenkov, Nevanlinna functions with real zeros, *Illinois J. Math.* 49 (2005) 1093–1110.
- [8] D. Masoero, Y-System and Deformed Thermodynamic Bethe Ansatz, arXiv:1005.1046.
- [9] R. Nevanlinna, Über Riemannsche Flächen mit endlich vielen Windungspunkten, *Acta Math.* 58 (1932) 295–373.
- [10] K. Shin, All cubic and quartic polynomials  $P$  for which  $f'' + P(z)f = 0$  has a solution with infinitely many real zeros and at most finitely many non-real zeros, Abstracts AMS 1057-34-26 (Lexington, KY, March 27-28, 2010).
- [11] Y. Sibuya, Global theory of a second order linear ordinary differential equation with a polynomial coefficient, North Holland, Amsterdam, 1975.



- [12] L. Volkovyski, Converging sequences of Riemann surfaces, *Mat. Sbornik*, 23 (65) N3 (1948) 361–382.

*Department of Mathematics  
Purdue University  
West Lafayette, IN 47907  
eremenko@math.purdue.edu  
agabriel@math.purdue.edu*